Journal of Electronic Materials (2023) 52:477–482
https://doi.org/10.1007/s11664-022-10015-z

ORIGINAL RESEARCH ARTICLE

Two-Dimensional Nodal-Loop Semimetal in Monolayer Zn_4C_2

Qian Xia[1] · Qiang Cao[1] · Sheng-Shi Li[1] · Wei-Xiao Ji[1]

Received: 6 September 2022 / Accepted: 3 October 2022 / Published online: 5 November 2022

Abstract
Nodal-loop semimetals are novel quantum materials that have attracted considerable research interest from scholars for their fascinating properties due to the band crossing characteristic. Nevertheless, nodal loop semimetals in two-dimensional (2D) lattices are quite rare. Here, we report our new discovery of a Zn_4C_2 monolayer with a P4/mmm symmetry tetragonal lattice that possesses a robust Dirac nodal-loop state, using first-principles calculations. Further calculations show that the gapless nodal-loop is protected by the horizontal mirror symmetry, which can be well maintained at external strains between -8% and 8%, and is also robust against the choice of U_{eff} for correlation effect and the choice of functional. The results of this paper reveal a new type of novel 2D Dirac nodal-loop material, which provides a new potential material for high-speed electronic devices.

Keywords First-principles calculations · nodal-loop · semimetal

Introduction

Since the discovery of graphene, two-dimensional (2D) materials have been of enormous curiosity to scholars.[1–4] Many of the exciting physical features of graphene are related to its topological band structure, i.e., the conduction and valence bands of graphene cross linearly on the Fermi surface in the Brillouin zone (BZ) to form a Dirac cone, which allows low-energy electrons to form similar two-dimensional massless Dirac fermions.[5] With the rapid development of experimental technology, in recent years, many new 2D materials have been synthesized experimentally,[2–4] and due to the discovery of the novel properties of graphene, there has been great enthusiasm for exploring 2D materials with nonlinear band topology.

After intensive research, more 2D materials with topological properties have been discovered, among which are topological semimetals. As an exciting ingredient for simulating quasiparticles in high-energy physics, topological semimetals have attracted much attention in condensed matter physics.[6–11]

The topological semimetals so far known can be categorized into Dirac semimetals,[9,10,12,13] Weyl semimetals,[14–16] nodal line semimetals,[17–20] and nodal surface semimetals.[21,22]All of these have non-trivial topological energy band structures near the Fermi surface, or symmetry-protected linear crossings of the energy bands. For Dirac semimetals, the energy band crossings are zero dimension, i.e., 0D, nodal points, and the points are isolated in the BZ, where they are normally protected by mirror symmetry, rotational symmetry, or glide mirror symmetry. Due to the fascinating physical characteristics of the low-energy excitation in this kind of semimetal, e.g., Fermi arcs surface states[23,24] and chiral anomalies,[25,26] they offer great application prospects for high-speed electronics.[27] A nodal-loop semimetal with one-dimensional (1D) properties forms a closed line that is always protected by chiral, mirror, and gliding mirror symmetries. Apart from applications in high-performance devices,[30] this property gives this peculiar semimetal a drumhead flat surface state,[28,29] which provides an essential platform for the implementation of intense electron correlation effects. The number of predicted 2D Dirac nodal states is very limited, with structures such as MnN, Si-Cmma, B_2O, B_6O, K_2N, $Cr_2N_6C_3$, and $TaSiTe_6$.[31–34] Among these, a few Dirac materials, such as Cu_2Si,[35] CuSe,[36] and $GdAg_2$[37] monolayers, have been verified. Therefore, the search for

✉ Qiang Cao
sdy_caoq@ujn.edu.cn

✉ Sheng-Shi Li
sdy_liss@ujn.edu.cn

[1] Spintronics Institute and School of Physics and Technology, University of Jinan, Jinan 250022, Shandong, People's Republic of China

non-trivial topological states, especially nodal-loop states, is still of great research value.

In this work, we carried out electronic band structure calculations to demonstrate that a 2D monolayer Zn_4C_2 is a symmetry-protected NL semimetal material, with the NL protected by horizontal mirror symmetry in the absence of spin–orbit coupling (SOC). The NL states hold steady against the uniaxial strains, and are independent of the choice of the correlation parameter, U_{eff} , and the choice of functional. Our results provide a new robust candidate of 2D nodal-loop semimetal material.

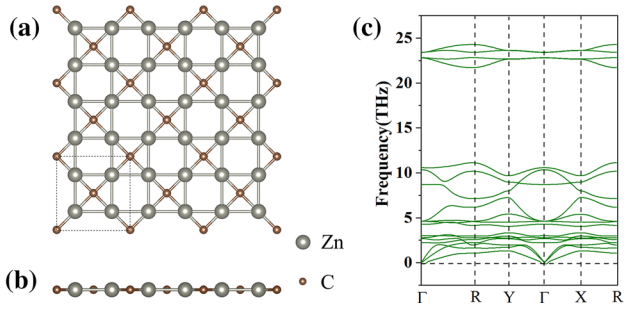

Fig. 1 (a) Top and (b) side views of Zn_4C_2, (c) the phonon dispersion spectrum of Zn_4C_2.

Computational Details

Our structural optimization and properties have been calculated by first-principles calculations based on a density functional theory (DFT) approach implemented in the Vienna Ab initio Simulation Package.[38,39] A vacuum space of 20 Å was set up to prevent interactions between neighboring atomic layers whose periodic images can be neglected. The generalized gradient approximation was used in the Perdew–Burke–Ernzerhof (PBE)[40] scheme to depict the exchange–correlation functional, various Hubbard U values were tested, and the results show that the properties are similar. So, we set $U_{\text{eff}} = 7.5$ eV to resolve the on-site Coulomb interactions in the d orbitals of the Zn atoms. The wave function was extended using a kinetic cutoff energy of 550 eV. The BZ was summarized by an 11 × 11 × 1 Γ-centered Monkhorst–Pack k-point grid. The lattice constants of the structures and the ionic positions of each atom were confirmed through structural full optimization until the energy converged to less than 10^{-7} eV and the force converged to less than 0.001 eV/Å. To verify the stability of the structure, the phonon dispersion spectrum was obtained using the PHONOPY code. The ab initio molecular dynamics (AIMD) simulations were performed based on Nose–Hoover canonical thermostat.

Results and Discussion

Figure 1a and b shows the atomic structure predicted in this work. The structure has a tetragonal lattice with P4/mmm symmetry and an optimized lattice constant of $a = b = 5.30$ Å, and each unit cell consists of four Zn atoms and two C atoms, with each C atom coordinated by four Zn atoms. The bond length of Zn-C was optimized to be 1.87 Å.

The cohesive energy of the quantity Zn_4C_2 was calculated first to prove its stability, and the equation for the cohesive energy is:

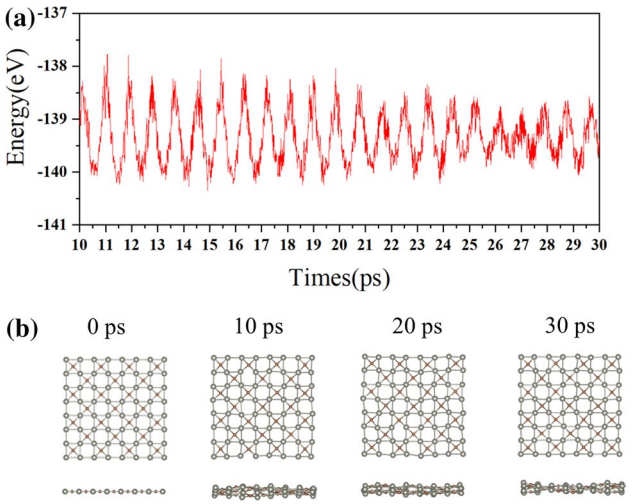

Fig. 2 (a) Total energy evolution of Zn_4C_2 monolayer at 300 K during AIMD simulation, (b) geometric structure snapshots of Zn_4C_2 monolayers in AIMD simulations at 0 ps, 10 ps, 20 ps, and 30 ps.

$$E_c = \left(4E_{Zn} + 2E_C - E_{Zn4C2}\right)/6,$$

in which the E_{Zn} and E_c represent the energies of Zn and C atom, respectively, and the E_{Zn4C2} represents the energy of Zn_4C_2. The cohesive energy of Zn_4C_2 is 2.149 eV/atom, slightly smaller than that of Cd_4C_2 (2.46 eV/atom) with similar configuration, as reported previously,[41] suggesting a moderately strong 2D bonded network, which is feasible for the experimental realization.

Furthermore, to verify the lattice dynamic and thermal stabilities of Zn_4C_2, we performed calculations on the phonon dispersion spectrum and AIMD simulations using a 3 × 3 supercell. The results of the phonon dispersion spectrum are shown in Fig. 1c. It can be seen that Zn_4C_2 is free of imaginary modes, demonstrating its dynamical stability. From the AIMD simulations, it can be seen that the total energy of the Zn_4C_2 monolayer fluctuates smoothly at 300 K, as shown in Fig. 2a. Figure 2b illustrates snapshots of the structures at 0 ps, 10 ps, 20 ps, and 30 ps, while no lattice

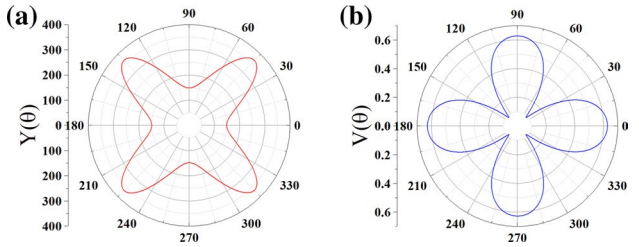

Fig. 3 (a, b) Young's modulus and Poisson's ratio of Zn_4C_2 monolayer.

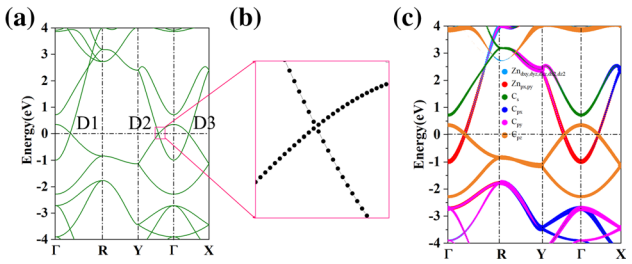

Fig. 4 (a) Electronic band structure at high symmetry points in the first BZ obtained by the PBE + U method, (b) partially amplified energy band structure diagram of Zn_4C_2 with increasing density of dots in the BZ at the second Dirac point, (c) corresponding orbital-resolved projection.

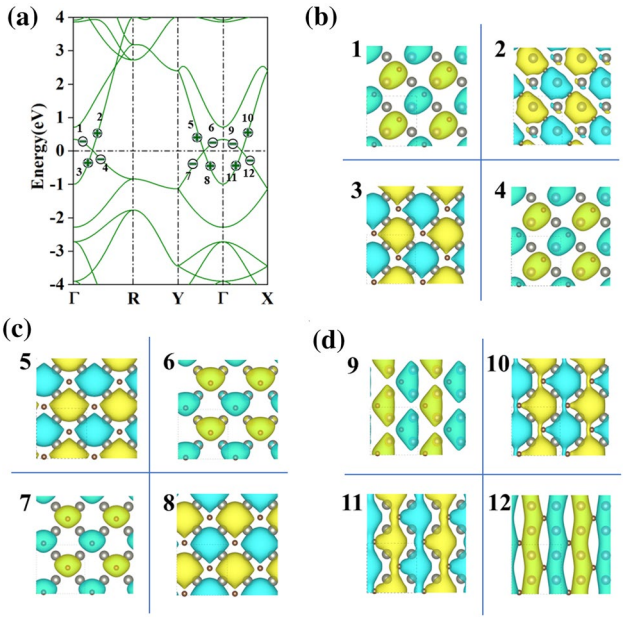

Fig. 5 (a) Calculated band structure of Zn_4C_2 monolayer, (b–d) real part of Kohn–Sham wave functions near each band crossing point.

deformation occurred, which demonstrates the thermally stability at room temperature.

The study then focused on the mechanical properties of the Zn_4C_2 monolayers. Their corresponding elastic constants were computed as $C_{11} = 245.08$ N/m, $C_{12} = 153.93$ N/m, $C_{22} = 245.08$ N/m, and $C_{44} = 168.53$ N/m. They well satisfy the Born–Huang criterion[42] ($C_{11} > 0$, $C_{11}C_{22} > {C_{12}}^2$, and $C_{44} > 0$). Taking this into account, the in-plane Young's modulus and the in-plane Poisson's ratio along any azimuthal angle ϕ can be computed using:

$$Y(\theta) = \frac{C_{11}C_{22} - C_{12}^2}{C_{11}s^4 + C_{22}c^4 + \left(\frac{C_{11}C_{22}-C_{12}^2}{C_{44}} - 2C_{12}\right)c^2s^2}$$

$$v(\theta) = -\frac{\left(C_{11} + C_{22} - \frac{C_{11}C_{22}-C_{12}^2}{C_{44}}\right)c^2s^2 - C_{12}\left(c^4 + s^4\right)}{C_{11}s^4 + C_{22}c^4 + \left(\frac{C_{11}C_{22}-C_{12}^2}{C_{44}} - 2C_{12}\right)c^2s^2},$$

where θ is the polar angle, $c = \cos\theta$ and $s = \sin\theta$. As plotted in Fig. 3a, we can see that the Young's modulus of Zn_4C_2 indicated a distinct anisotropy due to the quadrilateral symmetry. The maximum value of Young's modulus is about 364.97 N/m at $\theta = 45°$, and the minimum value is 62 N/m when $\theta = 0°$. The proportion of the maximum to the minimum value of the Young's modulus is about 5.87, this is further evidence of the significant anisotropy of the mechanical properties of Zn_4C_2. The behavior of the Poisson's ratio of Zn_4C_2 can be seen in Fig. 3b, which shows the exact opposite trend to the Young's modulus. The Young's modulus and the Poisson's ratio of the monolayer Zn_4C_2 structure are clearly orientation-dependent, which also demonstrates its anisotropic mechanical characteristics.

The DFT-based electronic band structure of Zn_4C_2 on the high symmetry path G-R-Y-G-X is plotted in Fig. 4a. Interestingly, the valence and conduction bands cross at the Fermi energy level and intersect at points, and we can see from Fig. 4a that these are along the G-R, G-Y, and G-X paths at three different points, D1, D2, and D3, respectively. Figure 4b plots a partial enlargement of the Fermi level band structure near point D2, which shows that the two bands exhibit a linear crossover property and that the charge carriers in them can be characterized as massless Dirac fermions. The more interesting discovery is that each energy band forming the Dirac cone corresponds to a well-defined orbital component, as shown in Fig. 4c, where crossings D1, D2, and D3 are dominated by p_{xy} of Zn and p_z of C, respectively.

The real part of Kohn–Sham wavefunctions near the three points are plotted in Fig. 5b to understand the mechanism of symmetric protection on the nodal-loop state. The space group of Zn_4C_2 is P4/mmm (No. 123), which includes 16 symmetry operators. Where all the path of high symmetry point $R - \Gamma$, $X - \Gamma$ and $Y - \Gamma$ in BZ are horizontal mirror-invariant high symmetry lines, the wavefunction on the two lines which are near the fermi level can be marked by the chiral eigenvalues (+ or −) of the mirror operator. By

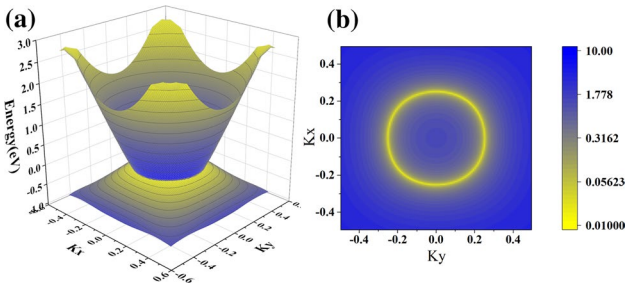

Fig. 6 (a) 3D band structure consisting of two energy bands closest to the Fermi surface, (b) in-plane projection of NL.

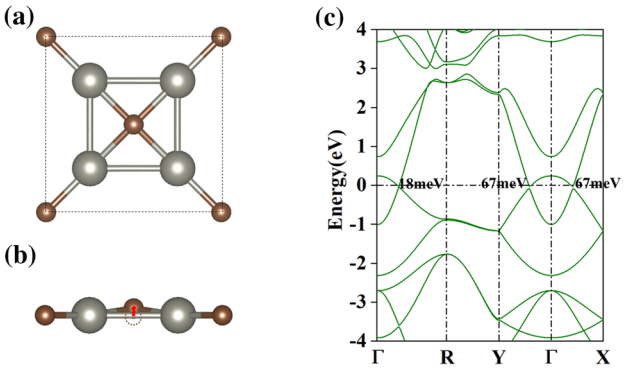

Fig. 7 (a) Top and (b) side views of geometric structure for distorted Zn_4C_2 monolayer; the brown dotted line represents the equilibrium position of the central C atom, (c) band structure of distorted Zn_4C_2 monolayer (Color figure online).

computing the eigenvalues about the horizontal mirror symmetry near the Fermi surface shown in Fig. 5a, we find that the crossing two bands have opposite mirror eigenvalues at all the three Dirac points (D1, D2, and D3), indicating that the band crossing is indeed protected by horizontal mirror symmetry. To illustrate the distribution of the crossing points, we further plot the two crossing bands near the Fermi level in the whole BZ, as shown in Fig. 6a, b, and we can see that the two energy bands intersect to form a closed nodal-loop state in the center of the first BZ.

In order to verify the mechanism of symmetric protection, we introduced manually structural distortion, as shown in Fig. 7a, b, in which the horizontal mirror symmetry is broken by shifting the equilibrium position of one C atom. The result shows that the NL states are eliminated due to the open of band gap at all the three band crossings (18 meV, 67 meV, and 67 meV for D1, D2, and D3, respectively). In conclusion, mirror symmetry plays a major role in the NL state of Zn_4C_2 protection.

Since strain is an effective means of regulating the electronic properties of 2D materials, we then further investigated whether the NL state can remain stable for different uniaxial strains without breaking the horizontal mirror

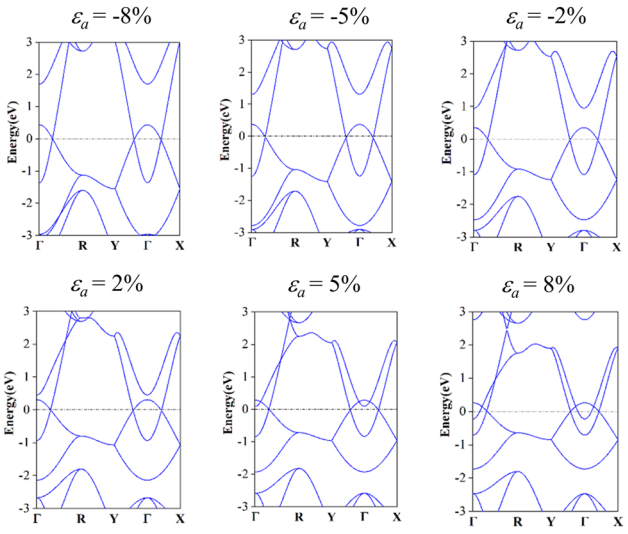

Fig. 8 Band structure obtained for Zn_4C_2 monolayer under uniaxial strain along the *a* direction.

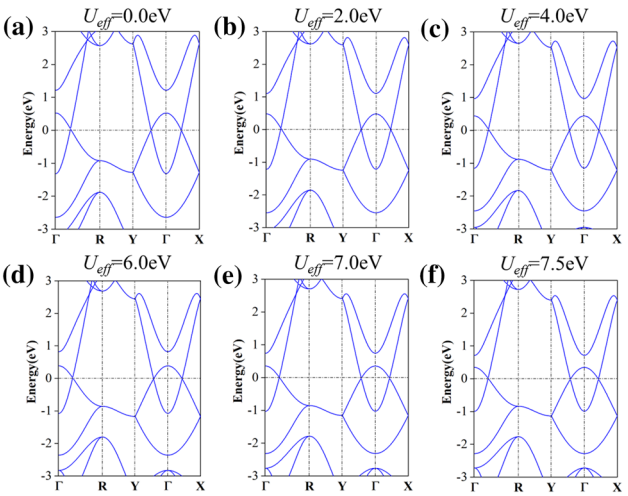

Fig. 9 (a–f) Calculated band structure of Zn_4C_2 monolayer with different U_{eff} values.

symmetry. Here, the strain is defined as $\varepsilon_a = (a - a_0)/a_0$ and $\varepsilon_b = (b - b_0)/b_0$, and we can vary the lattice constant to achieve strain engineering, while the energy band structure of Zn_4C_2 is well preserved in the strain. Figure 8 shows the energy band structure at six different strains, where the NL state is well protected due to the persistence of horizontal mirror symmetry.

Due to the correlation effect of transition metals possibly having an impact on the properties of the material, we used different U_{eff} values to check the band structure of Zn_4C_2. When the correlation effect is excluded ($U_{\text{eff}} = 0$), there are still three band crossings near the Fermi level, which indicates that the nodal-loop state is intrinsically present (see

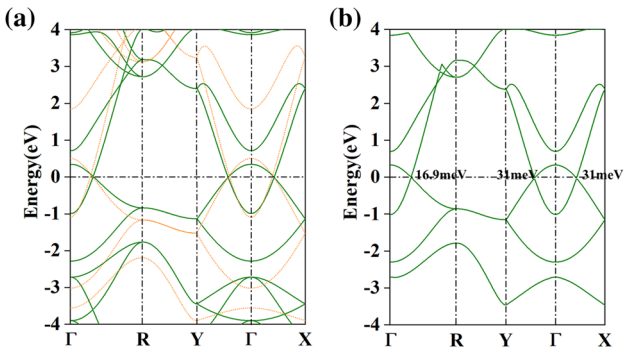

Fig. 10 (a) Band structure of Zn_4C_2 monolayer calculated with PBE + U (green solid line, $U = 7.5$ eV) and HSE06 (yellow dashed line) functions, (b) calculated band structure with SOC effect (Color figure online).

Fig. 9a). The NL state is maintained at different given values of U_{eff}, which indicates good robustness of NL against correlation effects, as shown in Fig. 9b–f. In addition, the band structure calculated by the HSE06 hybrid function further proves the existence of the NL state, which is similar to the band structure under $U_{\text{eff}} = 7.5$ eV, as shown in Fig. 10a, which indicates that the NL has good robustness against the choice of functional.

When the effect of SOC is taken into account, as shown in Fig. 10b, all three points at the Fermi level are open to varying degrees of band gaps. This is because the spin taken into account breaks the horizontal mirror symmetry of the wavefunction, which leads to the elimination of orbital orthogonality and the band crossing. However, since the energy band near the Fermi energy level is mainly contributed by the 3d orbitals of the Zn atoms, the SOC strength is relatively weak and the band gaps due to the SOC are tiny (16.9 meV, 31 meV, and 31 meV for D1, D2, and D3, respectively). In principle, such a narrow band gap opening does not seriously affect the application of the Zn_4C_2 monolayer at room temperature.

Conclusions

We have proposed a 2D Zn_4C_2 monolayer with the nodal-loop band state using first-principles calculations. This Zn_4C_2 film has good kinetic and thermal stability and is expected to be synthesized experimentally at room temperature. Notably, the nodal-loop state is protected by the horizontal mirror symmetry, making the nodal-loop gapless under different correlation effects and the choice of functional. Also, the nodal-loop state is robust against the uniaxial strain engineering of ± 8%. Our findings reveal a new type of novel 2D Dirac nodal-loop material, and provide a new potential candidate for high-speed electronic devices.

Acknowledgments This work was supported by the National Natural Science Foundation of China (Grant No. 12004137), Shandong Provincial Natural Science Foundation (Grant No. ZR2020QA052), National Natural Science Foundation of China (Grant No. 11974145), Shandong Provincial Natural Science Foundation (Grant No. ZR2020ZD28).

Conflict of interest The authors declare that they have no conflict of interest.

References

1. K.S. Novoselov, A.K. Geim, S.V. Morozov, D.-E. Jiang, Y. Zhang, S.V. Dubonos, I.V. Grigorieva, and A.A. Firsov, Electric field effect in atomically thin carbon films. *Science* 306, 666 (2004).
2. S.Z. Butler, S.M. Hollen, L. Cao, Y. Cui, J.A. Gupta, H.R. Gutiérrez, T.F. Heinz, S.S. Hong, J. Huang, and A.F. Ismach, Progress, challenges, and opportunities in two-dimensional materials beyond graphene. *ACS Nano* 7, 2898 (2013).
3. G.R. Bhimanapati, Z. Lin, V. Meunier, Y. Jung, J. Cha, S. Das, D. Xiao, Y. Son, M.S. Strano, and V.R. Cooper, Recent advances in two-dimensional materials beyond graphene. *ACS Nano* 9, 11509 (2015).
4. K. Novoselov, O.A. Mishchenko, and O.A. Carvalho, 2D materials and van der Waals neterostructures. Neto AC. *Science* 353, 6298 (2016).
5. A.C. Neto, F. Guinea, N.M. Peres, K.S. Novoselov, and A.K. Geim, The electronic properties of graphene. *Rev. Mod. Phys.* 81, 109 (2009).
6. N. Armitage, E. Mele, and A. Vishwanath, Weyl and Dirac semimetals in three-dimensional solids. *Rev. Mod. Phys.* 90, 015001 (2018).
7. A. Bansil, H. Lin, and T. Das, Colloquium: topological band theory. *Rev. Mod. Phys.* 88, 021004 (2016).
8. C.-K. Chiu, J.C. Teo, A.P. Schnyder, and S. Ryu, Classification of topological quantum matter with symmetries. *Rev. Mod. Phys.* 88, 035005 (2016).
9. A. Burkov, Giant planar hall effect in topological metals. *Phys. Rev. B* 96, 041110 (2017).
10. H. Weng, X. Dai, and Z. Fang, Topological semimetals predicted from first-principles calculations. *J. Phys. Condes. Matter* 28, 303001 (2016).
11. A. Burkov, Topological semimetals. *Nat. Mater.* 15, 1145 (2016).
12. Z. Wang, Y. Sun, X. Chen, C. Franchini, G. Xu, H. Weng, X. Dai, and Z. Fang, Dirac semimetal and topological phase transitions in A_3Bi (A = Na, K, Rb). *Phys. Rev. B* 85, 2202 (2012).
13. Z. Wang, H. Weng, Q. Wu, X. Dai, and Z. Fang, Three-dimensional Dirac semimetal and quantum transport in Cd_3As_2. *Phys. Rev. B* 88, 125427 (2013).
14. X. Wan, A.M. Turner, A. Vishwanath, and S.Y. Savrasov, Topological semimetal and fermi-arc surface states in the electronic structure of pyrochlore iridates. *Phys. Rev. B* 83, 205101 (2011).
15. G. Xu, H. Weng, Z. Wang, X. Dai, and Z. Fang, Chern semimetal and the quantized anomalous hall effect in $HgCr_2Se_4$. *Phys. Rev. Lett.* 107, 186806 (2011).
16. Y. Chen, Y. Xie, S.A. Yang, H. Pan, F. Zhang, M.L. Cohen, and S. Zhang, Nanostructured carbon allotropes with Weyl-like loops and points. *Nano Lett.* 15, 6974 (2015).
17. Y. Du, X. Bo, D. Wang, E.-J. Kan, C.-G. Duan, S.Y. Savrasov, and X. Wan, Emergence of topological nodal lines and type-II Weyl

nodes in the strong spin-orbit coupling system InNb X_2 (X = S, Se). *Phys. Rev. B* 96, 235152 (2017).
18. Y. Kim, B.J. Wieder, C. Kane, and A.M. Rappe, Dirac line nodes in inversion-symmetric crystals. *Phys. Rev. Lett.* 115, 036806 (2015).
19. S.-Y. Yang, H. Yang, E. Derunova, S.S. Parkin, B. Yan, and M.N. Ali, Symmetry demanded topological nodal-line materials. *Adv. Phys. X* 3, 1414631 (2018).
20. C. Fang, H. Weng, X. Dai, and Z. Fang, Topological nodal line semimetals. *Chin. Phys. B* 25, 117106 (2016).
21. Q.-F. Liang, J. Zhou, R. Yu, Z. Wang, and H. Weng, Node-surface and node-line fermions from nonsymmorphic lattice symmetries. *Phys. Rev. B* 93, 085427 (2016).
22. W. Wu, Y. Liu, S. Li, C. Zhong, Z.-M. Yu, X.-L. Sheng, Y. Zhao, and S.A. Yang, Nodal surface semimetals: theory and material realization. *Phys. Rev. B* 97, 115125 (2018).
23. I. Belopolski, K. Manna, D.S. Sanchez, G. Chang, B. Ernst, J. Yin, S.S. Zhang, T. Cochran, N. Shumiya, and H. Zheng, Discovery of topological Weyl fermion lines and drumhead surface states in a room temperature magnet. *Science* 365, 1278 (2019).
24. S.-Y. Xu, I. Belopolski, N. Alidoust, M. Neupane, G. Bian, C. Zhang, R. Sankar, G. Chang, Z. Yuan, and C.-C. Lee, Discovery of a Weyl fermion semimetal and topological Fermi arcs. *Science* 349, 613 (2015).
25. M. Hirschberger, S. Kushwaha, Z. Wang, Q. Gibson, S. Liang, C.A. Belvin, B.A. Bernevig, R.J. Cava, and N.P. Ong, The Chiral anomaly and thermopower of Weyl fermions in the half-Heusler GdPtBi. *Nat. Mater.* 15, 1161 (2016).
26. T.D. Son and Z.B. Spivak, Chiral anomaly and classical negative magnetoresistance of Weyl metals. *Phys. Rev. B* 88, 104412 (2013).
27. J. Kumar, P. Kapoor, and P. Ahluwalia, Na_3Bi: a robust material offering Dirac electrons for device applications. *J. Electron. Mater.* 44, 3215 (2015).
28. H. Huang, J. Liu, D. Vanderbilt, and W. Duan, Topological nodal-line semimetals in alkaline-earth stannides, germanides, and silicides. *Phys. Rev. B* 93, 201114 (2016).
29. H. Weng, Y. Liang, Q. Xu, R. Yu, Z. Fang, X. Dai, and Y. Kawazoe, Topological node-line semimetal in three-dimensional graphene networks. *Phys. Rev. B* 92, 045108 (2015).
30. K. Kim, J. Seo, E. Lee, K.-T. Ko, B. Kim, B.G. Jang, J.M. Ok, J. Lee, Y.J. Jo, and W. Kang, Large anomalous hall current induced by topological nodal lines in a ferromagnetic van der Waals semimetal. *Nat. Mater.* 17, 794 (2018).
31. S.-S. Wang, Z.-M. Yu, Y. Liu, Y. Jiao, S. Guan, X.-L. Sheng, and S.A. Yang, Two-dimensional nodal-loop half-metal in monolayer MnN. *Phys. Rev. Mater.* 3, 084201 (2019).
32. C. Zhong, W. Wu, J. He, G. Ding, Y. Liu, D. Li, S.A. Yang, and G. Zhang, Two-dimensional honeycomb borophene oxide: strong anisotropy and nodal loop transformation. *Nanoscale* 11, 2468 (2019).
33. S. Li, Y. Liu, S.-S. Wang, Z.-M. Yu, S. Guan, X.-L. Sheng, Y. Yao, and S.A. Yang, Nonsymmorphic-symmetry-protected hourglass Dirac loop, nodal line, and dirac point in bulk and monolayer X_3SiTe_6 (X = Ta, Nb). *Phys. Rev. B* 97, 045131 (2018).
34. L. Jin, X. Zhang, Y. Liu, X. Dai, X. Shen, L. Wang, and G. Liu, Two-dimensional Weyl nodal-line semimetal in a d^0 ferromagnetic K_2N monolayer with a high curie temperature. *Phys. Rev. B* 102, 125118 (2020).
35. R. Zhang, Z. Li, and J. Yang, Two-dimensional stoichiometric boron oxides as a versatile platform for electronic structure engineering. *J. Phys. Chem. Lett.* 8, 4347 (2017).
36. B. Feng, B. Fu, S. Kasamatsu, S. Ito, P. Cheng, C.-C. Liu, Y. Feng, S. Wu, S.K. Mahatha, and P. Sheverdyaeva, Experimental realization of two-dimensional Dirac nodal line fermions in monolayer Cu2Si. *Nat. Commun.* 8, 1 (2017).
37. B. Feng, R.-W. Zhang, Y. Feng, B. Fu, S. Wu, K. Miyamoto, S. He, L. Chen, K. Wu, and K. Shimada, Discovery of Weyl nodal lines in a single-layer ferromagnet. *Phys. Rev. Lett.* 123, 116401 (2019).
38. P. Blöchl, O. Jepsen, and O. Andersen, Improved tetrahedron method for Brillouin-zone integrations. *Phys. Rev. B* 49, 16223 (1994).
39. G. Kresse and D. Joubert, First-principles calculations of the vacancy formation energy in transition and noble metals. *Phys. Rev. B* 59, 1758 (1999).
40. J.P. Perdew, K. Burke, and M. Ernzerhof, Generalized gradient approximation made simple. *Phys. Rev. Lett.* 77, 3865 (1996).
41. L. Meng, S. Ni, Y. Zhang, B. Li, X. Zhou, and W. Wu, Two-dimensional zigzag-shaped Cd_2C monolayer with a desirable bandgap and high carrier mobility. *J. Mater. Chem. C* 6, 9175 (2018).
42. F. Mouhat, and F.-X. Coudert, Necessary and sufficient elastic stability conditions in various crystal systems. *Phys. Rev. B* 90, 224104 (2014).